Catalyst Stability

DOI: 10.1002/anie.201404103

Nanoparticle Growth in Supported Nickel Catalysts during Methanation Reaction—Larger is Better**

Peter Munnik, Marjolein E. Z. Velthoen, Petra E. de Jongh, Krijn P. de Jong, and Cedric J. Gommes**

Abstract: *A major cause of supported metal catalyst deactivation is particle growth by Ostwald ripening. Nickel catalysts, used in the methanation reaction, may suffer greatly from this through the formation of [Ni(CO)$_4$]. By analyzing catalysts with various particle sizes and spatial distributions, the interparticle distance was found to have little effect on the stability, because formation and decomposition of nickel carbonyl rather than diffusion was rate limiting. Small particles (3–4 nm) were found to grow very large (20–200 nm), involving local destruction of the support, which was detrimental to the catalyst stability. However, medium sized particles (8 nm) remained confined by the pores of the support displaying enhanced stability, and an activity 3 times higher than initially small particles after 150 h. Physical modeling suggests that the higher [Ni(CO)$_4$] supersaturation in catalysts with smaller particles enabled them to overcome the mechanical resistance of the support. Understanding the interplay of particle size and support properties related to the stability of nanoparticles offers the prospect of novel strategies to develop more stable nanostructured materials, also for applications beyond catalysis.*

Supported metal catalysts are of great importance for many processes related to the more sustainable production of fuels and chemicals.[1–6] Because the catalytic reactions take place on the surface of the active metal, the latter is generally dispersed in the form of nanoparticles, the size, shape and composition of which controls the activity and selectivity of the catalysts.[7–9] Much less is known about the relationship between a catalyst structure and its stability, even though it is pivotal to understand and to abate its irreversible deactivation.

[*] P. Munnik, M. E. Z. Velthoen, P. E. de Jongh, K. P. de Jong
Inorganic Chemistry and Catalysis
Debye institute for Nanomaterials Science, Utrecht University
Universiteitsweg 99, 3584 CG Utrecht (The Netherlands)
E-mail: k.p.dejong@uu.nl

C. J. Gommes
Department of Chemical Engineering, University of Liège
Allée du 6 Août 3, 4000 Liège (Belgium)
E-mail: cedric.gommes@ulg.ac.be

[**] The Netherlands Organization for Scientific Research is acknowledged for funding (NWO TOP 700.57.341) as well as the F.R.S.-FNRS (Belgium) for a Research Associate position to C.J.G. The Authors are grateful to Prof. G. W. Scherer (Princeton University) for discussions about the breaking of porous materials by confined nanoparticles.

Supporting information for this article is available on the WWW under http://dx.doi.org/10.1002/anie.201404103.

A major cause of catalyst deactivation is nanoparticle growth, a process thermodynamically driven by the high surface energy of the active metal. Nanoparticles may migrate over the support and coalesce to form larger particles. Alternatively Ostwald ripening may occur, whereby monoatomic species or small clusters diffuse from small to large particles.[10–13] Reactive gasses such as H_2, CO and H_2O, present in many industrial reactions, can accelerate growth of metal particles such as Pt, Pd, Co and Ni by lowering the diffusion barrier of whole particles through surface modification, or through the formation of mobile species such as metal carbonyls.[14–17] Recently, maximizing the distance between copper particles was shown to greatly stabilize catalysts for the synthesis of methanol.[18] Other factors that affect nanoparticle growth include the size, the composition as well as the metal–support interaction.[19–21] Here, we study how the particle spatial distribution and size affect the stability of supported nickel catalysts for methanation.

Nickel catalysts are often used for hydrogenation reactions such as that of CO into CH_4 and H_2O, for the production of synthetic methane or to remove CO from feed gasses of industrial ammonia plants.[22] In this process deactivation can occur by deposition of carbon on the active metal surface and by Ostwald ripening through the formation of [Ni(CO)$_4$] species.[23–27] The influence of the nickel particle size and spatial distribution on the nanoparticle stability remains poorly understood, which hampers the optimization of these catalysts.

Four catalysts with a nickel loading of ca. 20 wt.% were synthesized on the same silica gel support with different nickel particle sizes and different spatial distributions of the particles at the nanometer scale. This was achieved by varying the impregnation, drying and calcination methods (see Supporting Information) as previously reported in the literature.[28–32] The catalysts Ni-D8, Ni-C9, Ni-C4 and Ni-C3 were named by their volume-averaged Ni particle size (Figure 1 and Table 1).

The difference in spatial distribution was characterized quantitatively in terms of the percentage of support that was covered by nickel particles using low-magnification transmission electron microscopy (TEM) (Supporting Information, Figure S2). The coverage varied between 95% for Ni-D8 to 15% for Ni-C9, resulting in different surface-to-surface interparticle distances. For Ni-D8, particles were well dispersed (indicated with a D) with an average distance of 16 nm between nearest neighbors. In Ni-C9, Ni-C4 and Ni-C3, particles were closer (indicated with a C) with a distance of 7 nm (Table 1 and Supporting Information).

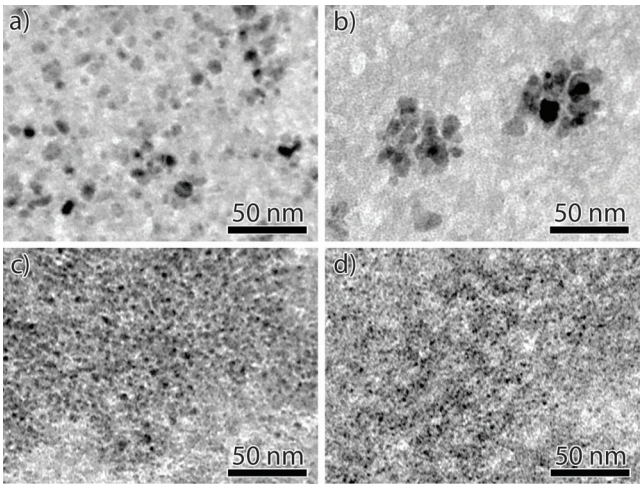

Figure 1. Bright-field TEM of 50 nm thick slices of Ni/SiO_2 catalysts after reduction: a) Ni-D8, b) Ni-C9, c) Ni-C4, and d) Ni-C3.

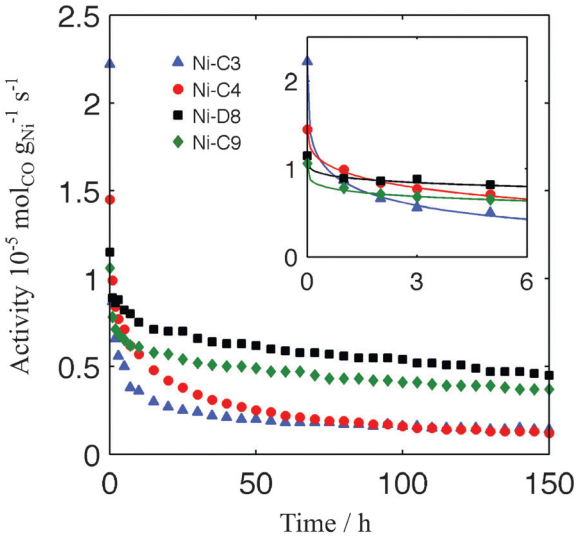

Figure 2. Nickel weight-based activity during 150 h on-stream at 230 °C with a H_2/CO feed ratio of 2:1. The inset is a close-up of the first 6 h.

Each catalyst was tested for the methanation reaction (230 °C, H_2:CO = 2:1, 1 bar). The gas hourly space velocity was chosen high enough to keep the conversion below 1 %, ensuring differential and isothermal conditions, and low enough to prevent significant loss of nickel from the reactor.[26,27] The conservation of nickel was also confirmed by energy dispersive X-ray spectroscopy (EDX) and calculations (see Supporting Information and Table S1). Note that under these reaction conditions the rate-determining step of the methanation is the hydrogenation of surface carbon species, so that the overall reaction is structure insensitive.[24,33,34]

Figure 2 shows the nickel weight-based activities of the catalysts. The initial activity, the activity after 150 h and the second-order deactivation constants are summarized in Table 1. The initial activities of the four catalysts were proportional to the surface area of the metal, with an average turnover frequency (TOF) of 4×10^{-3} s^{-1} (Figure S5). After 150 h, Ni-C9 and Ni-D8 both lost 60–65 % of their activity with similar deactivation rate constants, despite different interparticle distances. On the other hand, Ni-C4 and Ni-C3 both lost 90-95 % of their initial activity. It therefore appeared that the deactivation was controlled by the particle size rather than by the interparticle distance. After 150 h, the activity of the catalysts with small particles was three times lower than that of the catalysts with medium sized particles, which were more active in the long term. The observation that interparticle distance has no effect on the deactivation suggests that Ostwald ripening is the dominant mechanism for particle growth rather than migration and coalescence. This is in line with earlier observations that in presence of CO, migration and coalescence is significant only at temperatures above 500 °C, where nickel carbonyl species are unstable.[35–37]

The main intermediate species in Ostwald ripening is nickel carbonyl, which may exist both as an adspecies and as a gaseous molecule.[27] Independently of its dominant physical form, the equilibrium pressure of the carbonyl depends on the particle radius R according to the following Kelvin-like equation

$$P_{[Ni(CO)_4]} = K_0 \exp(\lambda/R) P_{CO}^4 \quad (1)$$

where K_0 is the equilibrium constant over a flat nickel surface, P_{CO} is the partial pressure of CO, and $\lambda = 3.9$ nm under the reaction conditions (see Supporting Information). Using these values and a conservative estimate for the diffusion coefficient of $[Ni(CO)_4]$ between two nanoparticles, the lifetime of 3 to 9 nm particles was found to be of the order of milliseconds to seconds, much shorter than the observed deactivation time. Thus, it is not diffusion but the formation

Table 1: Structural and catalytic properties of silica-supported nickel catalysts.

Catalyst	NiO crystallite size (XRD)[a] [nm]	Ni particle size (TEM)[b] [nm]	Nickel coverage[c] [%]	Interparticle distance[d] [nm]	Initial activity [10^{-5} mol_{CO} g_{Ni}^{-1} s^{-1}]	Activity after 150 h on-stream [10^{-5} mol_{CO} g_{Ni}^{-1} s^{-1}]	Deactivation constant[e] [10^{-2} h^{-1}]
Ni-D8	7.7	7.5	95 (±5)	16.0	1.1	0.46	2.5
Ni-C9	8.7	9.0	15 (±5)	7.1	1.0	0.35	2.7
Ni-C4	3.9	4.3	55 (±5)	6.9	1.5	0.12	9.0
Ni-C3	3.2	3.2	95 (±5)	6.8	2.2	0.14	29

[a] Volume average from XRD after calcination. [b] Volume average from TEM histogram analysis after reduction. [c] Percentage of support covered with nickel particles (Figure S2). [d] Nearest surface-to-surface distance calculated from the nickel loading, particle size, pore volume and nickel coverage assuming hexagonal packing. [e] Second-order deactivation rate constant (see Supporting Information).

and decomposition of the nickel carbonyl that controls the rate of Ostwald ripening. This explains why the spatial distribution of the nanoparticles only played a minor role in the deactivation and justifies using a mean-field approximation, in which the nickel carbonyl concentration is uniform throughout the catalyst.[12,17,38]

From metallurgy, the decomposition of nickel carbonyl is known to proceed through competitive adsorption of carbonyl and carbon monoxide on the nickel surface, followed by the successive chemisorption of the carbonyl groups on neighboring empty surface sites.[39] From transition-state theory, the time-evolution of the radius of a spherical nickel particle obeys

$$\frac{dR}{dt} = \nu(S - \exp(\lambda/R)) \qquad (2)$$

where ν is a velocity that depends on the kinetic constants of the reaction as well as on the partial pressure of CO, which was estimated at $\nu = 0.87\ \mathrm{nm\,h^{-1}}$ from literature data (Supporting Information).[40] S is the nickel carbonyl supersaturation ratio defined as $P_{Ni(CO)_4}/(K_0 P_{CO}{}^4)$. Equation (2) assumes unhindered growth, so that the particles are free to grow larger than the pores of the support, which has notably been observed for noble metals in zeolites.[41,42] The value of the supersaturation S is calculated as the area-weighted average of the Kelvin-like factor $\exp(\lambda/R)$ calculated over all the particles, which ensures nickel conservation (Supporting Information).

Figure 3 compares the experimental activities of Ni-C3 and Ni-D8 with the predictions of Equation (2), assuming an activity proportional to the surface area of the nanoparticles with the TOF measured on the fresh catalysts (solid blue lines) or on the spent catalysts (dashed blue lines). The deactivation of Ni-C3 was well accounted for by the unhindered Ostwald ripening model, limited by the rate of formation and decomposition of nickel carbonyl. Interestingly, in the case of Ni-D8, the experimental deactivation was much slower than predicted by the present model. Similar conclusions hold when comparing Ni-C4 to Ni-C9 (Figure S13).

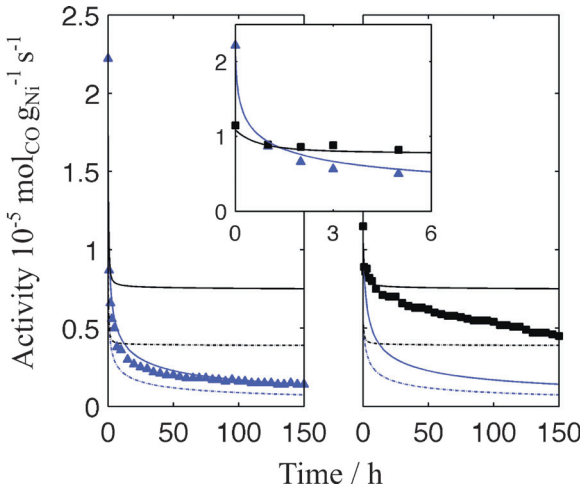

Figure 3. Modelling the deactivation of catalysts Ni-C3 (left) and Ni-D8 (right). The symbols represent the experimental data, the lines the model predictions: unhindered particle growth (blue) and confined growth (black). The solid and dashed lines are obtained using the TOF of the fresh and spent catalysts, respectively, which accounts for carbon buildup. The initial particle size distribution played a large role only in the first hour of the modelling predictions (Figure S11). In the inset, the unhindered growth model is used for Ni-C3 and the confined model for Ni-D8.

Figure 4 shows TEM of the catalysts after 150 h on-stream, and the particle size distributions derived from TEM are presented in Figure S4. A remarkable feature of Ni-C4 and Ni-C3 is the presence of particles that can be as large as 100 nm (Figure S4). In both cases, the volume-averaged particle size is around 20 nm (Table S1), much larger than the 10 nm pore size of the support. Studying a Ni/SBA-15 catalyst with 4 nm initial Ni particles for comparison, electron tomography confirmed that similar large nickel particles had grown much larger than the pores of the support, locally breaking up the silica walls to do so (Figures S6 and S7). These results show that the unhindered growth mechanism is a valid assumption for catalyst with initially small particles. By contrast, Ni-D8 and Ni-C9 exhibited only a minor increase in particle size, from 7.5 to 9.0 nm and 9.0 to 11.1 nm, respectively, suggesting that the particles were confined in the pores (Figure S4).

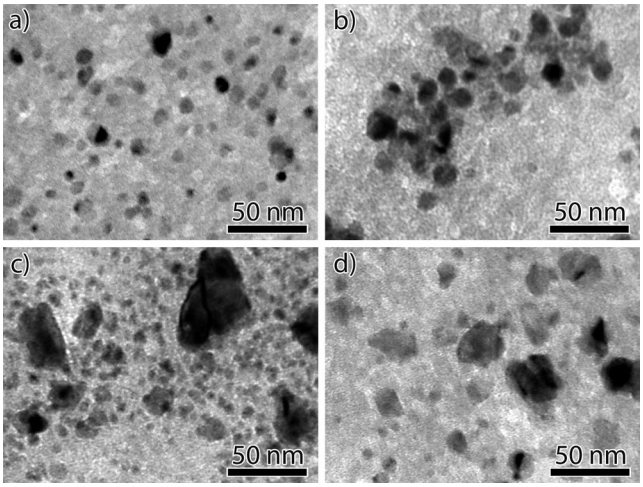

Figure 4. TEM of microtomed 50 nm slices of catalyst particles after 150 h on-stream. a) Ni-D8, b) Ni-C9, c) Ni-C4, and d) Ni-C3.

The conditions for a growing nanoparticle to break a pore wall or to be confined by it is a problem familiar to engineers interested in the weathering of construction materials.[43] The quantitative criteria depend on the specific microstructure of the material, its mechanical properties, and the surface energies of the interfaces.[44] Qualitatively, however, the criterion is universal: if the supersaturation of the reservoir from which the nanoparticle grows is high enough, the free energy released by the growth is sufficient to overcome the mechanical resistance of the confining material. In the present context, the supersaturation is controlled by the particle size according to the area-weighted average of $\exp(\lambda/$

R). The values calculated from the experimental size distributions of the fresh catalysts are $S = 19$ and 8 for Ni-C3 and Ni-C4, and $S = 3$ and 2.5 for Ni-D8 and Ni-C9. The absence of very large particles in Ni-D8 and Ni-C9 suggests that the critical value of the supersaturation for the silica gels used in the present work lies between 3 and 8.

To further test the confinement of particles in Ni-C8 and Ni-D9, Equation (2) was solved again while limiting the growth of particles to the pore size, approximately 10 nm (see Supporting Information). The results are plotted as black lines in Figure 3. By contrast to Ni-C3, the activity of Ni-D8 was well accounted for by the confined growth model. The agreement was almost quantitative for short times, but the activity progressively dropped below the prediction of the confined model over 150 h. This was explained by carbon buildup on the nickel surface. Although the TOF did not depend on particle size, an approximately 50% reduction in TOF was apparent for all catalysts over 150 h (Figure S5). This suggests that unreactive carbon coated half of the nickel surface, in line with previous studies.[24,27,37] Using the initial and final TOF as upper and lower bounds (solid and dashed lines in Figure 3), the deactivation of Ni-C3 and Ni-D8 were well described by Equation (2); unhindered growth was dominant in the former, while confined growth applied to the latter.

A similar observation was made when considering the particle size distributions (Figures S4 and S12). The unhindered model was in fair agreement with the experimental particle size distributions of Ni-C3 and Ni-C4, but only the confined growth model could account for the particle stability in Ni-C9 and Ni-D8. Interestingly, the very large particles in Ni-C3 and Ni-C4 coexisted with smaller particles that were not predicted by the unhindered growth model (Figures 4 and S4). These results suggest that unhindered growth applied only for a short time during which the supersaturation was sufficiently high (Figure S13). This was followed by a hybrid regime where the particles smaller than the pores remained confined, while the larger particles grew unhindered. After a few hours, the average particle size of Ni-C3 reached the same value as Ni-D8 resulting in identical activities (inset of Figure 3). However, the presence of the few particles that broke early though the pores was responsible for the faster and more extensive deactivation of Ni-C3.

In conclusion, the stability of Ni/SiO_2 catalysts with different particle sizes and interparticle distances was studied during the methanation reaction. The distance between neighboring particles was found to have only a minor influence on the stability. The deactivation by Ostwald ripening was limited not by diffusion but by the formation and decomposition of nickel carbonyl on the metal surface. The main determinant of the catalyst stability was the particle size. Catalysts with smaller particles deactivated faster and to a larger extent than catalysts with medium sized particles. This counter-intuitive finding resulted from qualitatively different mechanisms. In the case of small particles, the nickel carbonyl supersaturation was sufficiently high for the particles to break the pore walls, resulting in very large nanoparticles. By contrast, the supersaturation was low in catalysts with medium sized nanoparticles, which limited the possible extent of their growth to the pore diameter. The large difference in stability between particles that differ only by a few nanometers in size is very relevant not only for durable catalysis, but also for other fields such as that of nanostructured materials for energy conversion and storage devices.[45]

Experimental Section

Detailed information on the catalyst synthesis and Ostwald ripening model can be found in the Supporting Information. For TEM, catalysts were embedded in an epoxy resin and cut in 50 nm slices by ultramicrotomy. This allowed the imaging of cross-sections of entire grains and the ability to look effectively inside the catalyst support particles, and all images shown were verified to be representable for the catalyst particle and other particles of the same sample.

Received: April 8, 2014
Revised: May 19, 2014
Published online: July 7, 2014

Keywords: crystal growth · heterogeneous catalysis · nanoparticles · nickel · supported catalysts

[1] Y. Román-Leshkov, C. J. Barrett, Z. Y. Liu, J. A. Dumesic, *Nature* **2007**, *447*, 982 – 985.
[2] S. Guo, S. Zhang, S. Sun, *Angew. Chem.* **2013**, *125*, 8686 – 8705; *Angew. Chem. Int. Ed.* **2013**, *52*, 8526 – 8544.
[3] V. R. Calderone, N. R. Shiju, D. Curulla-Ferré, S. Chambrey, A. Y. Khodakov, A. Rose, J. Thiessen, A. Jess, G. Rothenberg, *Angew. Chem.* **2013**, *125*, 4493 – 4497; *Angew. Chem. Int. Ed.* **2013**, *52*, 4397 – 4401.
[4] H. M. Torres Galvis, J. H. Bitter, C. B. Khare, M. Ruitenbeek, A. I. Dugulan, K. P. de Jong, *Science* **2012**, *335*, 835 – 838.
[5] C. Galeano, J. C. Meier, V. Peinecke, H. Bongard, I. Katsounaros, A. Topalov, A. Lu, K. J. J. Mayrhofer, F. Schüth, *J. Am. Chem. Soc.* **2012**, *134*, 20457 – 20465.
[6] A. S. Aricò, P. G. Bruce, B. Scrosati, J.-M. Tarascon, W. van Schalkwijk, *Nat. Mater.* **2005**, *4*, 366 – 377.
[7] J. P. den Breejen, P. B. Radstake, G. L. Bezemer, J. H. Bitter, V. Frøseth, A. Holmen, K. P. de Jong, *J. Am. Chem. Soc.* **2009**, *131*, 7197 – 7203.
[8] S. B. Simonsen, I. Chorkendorff, S. Dahl, M. Skoglundh, K. Meinander, T. N. Jensen, J. V. Lauritsen, S. Helveg, *J. Phys. Chem. C* **2012**, *116*, 5646 – 5653.
[9] F. Studt, F. Abild-Pedersen, T. Bligaard, R. Z. Sørensen, C. H. Christensen, J. K. Nørskov, *Science* **2008**, *320*, 1320 – 1322.
[10] T. W. Hansen, A. T. Delariva, S. R. Challa, A. K. Datye, *Acc. Chem. Res.* **2013**, *46*, 1720 – 1730.
[11] M. A. Newton, *Chem. Soc. Rev.* **2008**, *37*, 2644 – 2657.
[12] R. Ouyang, J.-X. Liu, W.-X. Li, *J. Am. Chem. Soc.* **2013**, *135*, 1760 – 1771.
[13] A. D. Benavidez, L. Kovarik, A. Genc, N. Agrawal, E. M. Larsson, T. W. Hansen, A. M. Karim, A. K. Datye, *ACS Catal.* **2012**, *2*, 2349 – 2356.
[14] G. S. Parkinson, Z. Novotny, G. Argentero, M. Schmid, J. Pavelec, R. Kosak, P. Blaha, U. Diebold, *Nat. Mater.* **2013**, *12*, 724 – 728.
[15] S. Horch, H. Lorensen, S. Helveg, E. Laegsgaard, I. Stensgaard, K. W. Jacobsenk, J. K. Norskov, F. Besenbacher, *Nature* **1999**, *398*, 134 – 136.
[16] M. Sadeqzadeh, J. Hong, P. Fongarland, D. Curulla-Ferré, F. Luck, J. Bousquet, D. Schweich, A. Y. Khodakov, *Ind. Eng. Chem. Res.* **2012**, *51*, 11955 – 11964.

[17] S. R. Challa, A. T. Delariva, T. W. Hansen, S. Helveg, J. Sehested, P. L. Hansen, F. Garzon, A. K. Datye, *J. Am. Chem. Soc.* **2011**, *133*, 20672 – 20675.
[18] G. Prieto, J. Zečević, H. Friedrich, K. P. de Jong, P. E. de Jongh, *Nat. Mater.* **2013**, *12*, 34 – 39.
[19] C. T. Campbell, S. Parker, D. Starr, *Science* **2002**, *298*, 811 – 814.
[20] A. Cao, G. Veser, *Nat. Mater.* **2010**, *9*, 75 – 81.
[21] J. A. Farmer, C. T. Campbell, *Science* **2010**, *329*, 933 – 936.
[22] J. Kopyscinski, T. J. Schildhauer, S. M. A. Biollaz, *Fuel* **2010**, *89*, 1763 – 1783.
[23] M. Mihaylov, K. Hadjiivanov, H. Knözinger, *Catal. Lett.* **2001**, *76*, 59 – 63.
[24] M. Agnelli, H. M. Swaan, C. Marquez-Alvarez, G. A. Martin, C. Mirodatos, *J. Catal.* **1998**, *175*, 117 – 128.
[25] W. M. Goldberger, D. F. Othmer, *Ind. Eng. Chem. Process Des. Dev.* **1963**, *2*, 202 – 209.
[26] W. M. Shen, J. A. Dumesic, C. G. Hill, *J. Catal.* **1981**, *68*, 152 – 165.
[27] M. Agnelli, M. Kolb, C. Mirodatos, *J. Catal.* **1994**, *148*, 9 – 21.
[28] T. M. Eggenhuisen, P. Munnik, H. Talsma, P. E. de Jongh, K. P. de Jong, *J. Catal.* **2013**, *297*, 306 – 313.
[29] J. R. A. Sietsma, J. D. Meeldijk, J. P. den Breejen, M. Versluijs-Helder, J. A. van Dillen, P. E. de Jongh, K. P. de Jong, *Angew. Chem.* **2007**, *119*, 4631 – 4633; *Angew. Chem. Int. Ed.* **2007**, *46*, 4547 – 4549.
[30] T. M. Eggenhuisen, J. P. den Breejen, D. Verdoes, P. E. de Jongh, K. P. de Jong, *J. Am. Chem. Soc.* **2010**, *132*, 18318 – 18325.
[31] T. M. Eggenhuisen, H. Friedrich, F. Nudelman, J. Zečević, N. A. J. M. Sommerdijk, P. E. de Jongh, K. P. de Jong, *Chem. Mater.* **2013**, *25*, 890 – 896.
[32] N. E. Bogdanchikova, V. V. Tretyakov, *Preparation of Catalysts V*, Elsevier, Amsterdam, **1991**.
[33] M. P. Andersson, F. Abild-Pedersen, I. N. Remediakis, T. Bligaard, G. Jones, J. Engbæk, O. Lytken, S. Horch, J. H. Nielsen, J. Sehested, *J. Catal.* **2008**, *255*, 6 – 19.
[34] I. Alstrup, *J. Catal.* **1995**, *151*, 216.
[35] J. Sehested, J. A. P. Gelten, S. Helveg, *Appl. Catal. A* **2006**, *309*, 237 – 246.
[36] B. M. Vogelaar, A. D. van Langeveld, P. J. Kooyman, C. M. Lok, R. L. C. Bonné, J. A. Moulijn, *Catal. Today* **2011**, *163*, 20 – 26.
[37] M. Agnelli, C. Mirodatos, *J. Catal.* **2000**, *192*, 204 – 214.
[38] S. Bredmose, I. Chorkendorff, S. Dahl, M. Skoglundh, J. Sehested, S. Helveg, *J. Catal.* **2011**, *281*, 147 – 155.
[39] A. P. Garratt, H. W. Thompson, *J. Chem. Soc.* **1934**, 1822 – 1825.
[40] H. E. Carlton, J. H. Oxley, *AIChE J.* **1967**, *13*, 86 – 91.
[41] J. Zečević, A. M. J. van der Eerden, H. Friedrich, P. E. de Jongh, K. P. de Jong, *ACS Nano* **2013**, *7*, 3698 – 3705.
[42] P. Gallezot, A. Alarcon-Diaz, J. A. Dalmon, A. J. Renouprez, B. Imelik, *J. Catal.* **1975**, *39*, 334 – 349.
[43] O. Coussy, *Mechanics and Physics of Porous Solids*, Wiley, Chichester, **2010**.
[44] G. W. Scherer, *Cem. Concr. Res.* **1999**, *29*, 1347 – 1358.
[45] E. F. Holby, W. Sheng, Y. Shao-Horn, D. Morgan, *Energy Environ. Sci.* **2009**, *2*, 865 – 871.

